Project 3: Volatility Dynamics Under the Heston Model

by

Austin Grier, Vanessa Pizante, Hersh Stark, Kevin Zhu

A project submitted in conformity with the requirements for STA2503
Graduate Department of Statistical Sciences
University of Toronto

November 21, 2018

Abstract

Project 3: Volatility Dynamics Under the Heston Model

Austin Grier, Vanessa Pizante, Hersh Stark, Kevin Zhu
STA2503
Graduate Department of Statistics
University of Toronto
2018

In this work we explore the Heston Model, a stochastic volatility model that can be used to explain the dynamic volatility skew observed in financial markets. We explore the effect of the Heston Model parameters in determining the nature of the skew, and explore various numerical discretization methods to simulate the paths of the volatility and asset price processes under the Heston Model. We use the simulated processes to obtain Monte Carlo Estimates of European options on assets with prices determined by the Heston Model and invert the Black-Scholes formula to obtain estimates of the implied volatility skew. We also use the framework to price variance swaps analytically and numerically, which we use as control variates to obtain a variance reduction for the estimated implied volatility skew.

Chapter 1

Introduction

In the Black-Scholes-Merton model, the volatility of an underlying asset of an option is assumed to be constant. Intutition and empirical market data contradict this constant-volatility notion, and it is therefore viewed as a major shortcoming of the model. The underlying asset's volatility is the only variable in the Black-Scholes option pricing formula that cannot be directly observed in the market. However, we can invert the Black-Scholes formula with respect to σ and use an observed option price to compute σ_{imp}, the implied volatility. Specifically $\sigma_{imp}(K,T)$ is the volatility that calibrates the market price with the Black-Scholes price. That is:

$$V^*(K,T;S_0) = V^{BS}(K,T,S_0,r,\sigma_{imp}(K,T))$$

where V^* is the observed market price of the option with strike K and expiry time T, and V^{BS} is the Black-Scholes option price for that same option. Under the Black-Scholes model, σ should be constant with respect to strike (K), maturity (T), and time (t), but empirical market data indicates that this is a poor assumption.

Practitioners who are aware of this issue generally begin by plotting implied volatilities versus strike price, which results in what is known as a 'volatility smile.' This is a consequence of in-the-money options tending to have lower implied volatilites than out-of-the-money options. There also tends to be asymmetry to this relationship, with lower strikes having higher implied volatilties for equities and higher implied volatilities at higher strikes for commodities leading to a 'volatility skew' rather than smile. This reflects the tendency of options with higher payoffs during adverse events to have more expensive market prices, and thus have higher implied volatilties. Many practitioners also go a step further and include tenor (T) in the plots, resulting in a 3-dimensional volatility surface. Contrary to Black-Scholes theory, empirical evidence clearly indicates that the surface is not constant and varies over time, suggesting the need for a model for σ that can capture the dynamic volatility skew.

To overcome this shortcoming, we can either allow σ to be a deterministic function of time and/or a stochastic process such as the asset price (a local volatility model), or we can allow σ itself to be driven by its own source of stochasticity (a stochastic volatility model). In this work, we choose to adopt the latter approach

using arguably the most popular stochastic volatility model in practice: the Heston Model.

Chapter 2

Mathematical Analysis

2.1 Model Set-up

In this project, we examine a continuous-time stochastic volatility model called the Heston model, in which an asset price and its volatility satisfy coupled stochastic dynamics. More precisely, the variance of the asset returns, $\nu = (\nu_t)_{t\geq 0}$ follows a Feller process (sometimes referred to as a CIR process) and the asset price follows an Ito Process with variance ν_t. The volatility process and asset price process $(S_t)_{t\geq 0}$ satisfy the following coupled SDE under the real-world measure $\mathbb{P}$:

$$dS_t = \mu S_t dt + S_t\sqrt{\nu_t}dW_t^{\mathbb{P}}, \quad d\nu_t = \kappa^{\mathbb{P}}(\theta^{\mathbb{P}} - \nu_t)dt + \eta\sqrt{\nu_t}dB_t^{\mathbb{P}} \tag{2.1}$$

where $W_t^{\mathbb{P}}$ and $B_t^{\mathbb{P}}$ are $\mathbb{P}$-Brownian motions with correlation ρ.

Assuming the risk-free interest rate r is 0 (an assumption we will continue with for the remainder of this work), it is easily shown that the corresponding risk-neutral dynamics of the model can be written as:

$$dS_t = S_t\sqrt{\nu_t}dW_t, \quad d\nu_t = \kappa(\theta - \nu_t)dt + \eta\sqrt{\nu_t}dB_s \tag{2.2}$$

where B and W are Brownian motions under $\mathbb{Q}$, the risk-neutral measure. Note that η is the volatility of the volatility (or vol-vol), θ is the long-run mean of the variance and κ is the rate at which ν_t returns θ. This provides a useful interpretation of θ, κ, and η as being the mean, mean-reverting rate, and volatility of ν_t, respectively.

We would now like to price a derivative with price process $g = (g_t)_{t\geq 0}$ and payoff $G(S_T, \nu_T)$, where $g_t = g(t, S_t, \nu_t)$ for some function g. Hence:

$$g_t = g(t, S_t, \nu_t) = \mathbb{E}_t^{\mathbb{Q}}G[(S_T, \nu_T)]$$

So by Feymann-Kac and (2.2), g satisfies the following PDE:

$$\begin{cases} (\partial_t + \mathcal{L}^{S,\ \nu})g = 0 \\ g(T, S, \nu) = G(S, \nu) \end{cases}$$

where $\mathcal{L}^{S,\nu} = \frac{1}{2}\nu S^2 \cdot \partial_{SS} + \kappa(\theta - \nu) \cdot \partial_\nu + \frac{1}{2}\eta^2\nu \cdot \partial_{\nu\nu} + \rho\eta\nu S \cdot \partial_{S\nu}$ is the infinitesimal generator of the process.

This PDE can be linearized by setting $X_t = \log(S_t)$. So now, using Ito's lemma, the $\mathbb{Q}$-dynamics of X and ν can be rewritten as:

$$dX_t = -\frac{1}{2}\nu_t dt + \sqrt{\nu_t}dW_t, \quad d\nu_t = \kappa(\theta - \nu_t)dt + \eta\sqrt{\nu_t}dB_s \tag{2.3}$$

Through a similar substitution, the derivative price process g_t can be written as

$$g_t = g(t, X_t, \nu_t) = \mathbb{E}_t^{\mathbb{Q}}[G(e^{X_T}, \nu_T)] \tag{2.4}$$

Thus, we can again employ Feymann-Kac to obtain the following affine PDE for g in terms of $x = \log S$:

$$\begin{cases} (\partial_t + \mathcal{L}^{X,\nu})g = 0 \\ g(T, X, \nu) = G(e^X, \nu) \end{cases}$$

where $\mathcal{L}^{X,\nu} = -\frac{1}{2}\nu \cdot \partial_x + \frac{1}{2}\nu \cdot \partial_{xx} + \kappa(\theta - \nu) \cdot \partial_\nu + \frac{1}{2}\eta^2\nu \cdot \partial_{\nu\nu} + \rho\eta\nu \cdot \partial_{x\nu}$ is the infinitesimal generator of the process.

Now that we have adequately set up a model for our problem, we can attempt to do the following:

- Obtain the values of some variance claims analytically
- Establish SDE discretization methods to numerically simulate the coupled process (ν_t, S_t)
- Use the simulated process (ν_t, S_t) to numerically price some variance claims and European call and put options using Monte Carlo methods
- Seek a variance reduction for the Monte Carlo methods of the European options, using variance claims as control variates.
- Compare the analytical and numerical valuations of the variance claims
- Use the numerical simulation techniques to estimate implied volatility skews
- Describe the effect of the Heston Model parameters on the volatility skews

We attempt to address the above points throughout the remainder of this work, not necessarily in the order presented above.

2.2 Estimating the Implied Volatility Smirk

Our objective is to estimate the implied volatility smirks derived from a set of European put and call options written on the same asset for various values of K and T. Note that we will use put options for strike prices $K < S_0$ and call options for $K \geq S_0$. This means that we will use out-of-the-money (OTM) options rather than in-the-money (ITM) options to estimate the volatility smirk. The argument favoring OTM options versus ITM options for volatility smirk estimation comes from a decomposition of an option price G into (1) forward intrinsic value, which is largely independent of volatility, and (2) time value, which is almost completely dependent on volatility: $G(S_t, \sigma) = G^{(Intr.)}(S_t) + G^{(Time)}(S_t, \sigma)$. The linearity of the expectation operator allows Monte-Carlo estimation error to be similarly decomposed as such. For ITM options, the intrinsic value tends to be greater than the time value and so a larger proportion of the estimation error can be attributed to the intrinsic value component. For OTM options, the intrinsic value is negligble, and so almost all of the estimation error is attributable to the time value, leading to a more precise overall estimate of option price and consequently implied volatility.

Thus we consider OTM options:

$$G(e^X, \nu) = \begin{cases} (e^X - K)_+ & \text{if } e^{X_0} \leq K \\ (K - e^X)_+ & \text{if } e^{X_0} > K \end{cases}$$

The option price at time t given in equation (2.4) can be approximated by Monte-Carlo estimation. Specifically, for M simulations of $X_T^{(m)}$ with M sufficiently large, we can numerically compute the Monte-Carlo estimate and its associated variance as:

$$g(t, x, \nu) \approx \hat{g}(t, x, \nu) = \frac{1}{M} \sum_{m=1}^{M} G\left(e^{X_T^{(m)}}\right) \tag{2.5}$$

$$\hat{\sigma_g^2} = \frac{1}{M-1} \sum_{m=1}^{M} \left(e^{X_T^{(m)}} - \hat{g}(t, x, \nu)\right)^2 \tag{2.6}$$

with associated $(1-\alpha)\%$ confidence interval given by:

$$P\left(g(t, x, \nu) \in \left[\hat{g}(t, x, \nu) \pm \frac{z_\alpha \sigma_g}{\sqrt{M}}\right]\right) = 1 - \alpha$$

where z_α is the appropriate critical value from a standard Gaussian distribution. In this work, we will use construct 95% confidence bands for the estimated volatility smirks. Once we obtain the Monte Carlo estimate and corresponding upper and lower confidence limits of the option price, we can invert the Black-Scholes formula as discussed previously to obtain an estimate of the implied volatility smirk and its associated "confidence smirks." Since there is no closed form for the inverted Black Scholes formula, we utilize a MINPACK solver [Garbow, 1980] to numerically obtain:

$$\sigma^{(Implied)} = \overset{\arg\min}{\sigma} V^{BS}(K, T, t, S_0, r, \sigma) - \hat{g}(t, x, v) \tag{2.7}$$

We can then repeat this process for various K and T to obtain a volatility smirk for each maturity. The remaining consideration is how to simulate X_T, as unlike in the standard Black-Scholes framework we do not have a simple lognormal form for the terminal asset value S_T. Instead, we can numerically approximate the coupled SDE on a grid to simulate the entire paths of both the volatility process and the asset price procsses, and utilize the terminal asset prices in the Monte-Carlo method just visited. In the implementation section of this work, we will visit three methods to numerically approximate the coupled SDE via discretization schemes.

2.3 Analytic Solutions using the Heston Model

Although an analytical solution for the Heston Model can be derived in closed-form via characterstic functions, we will not adopt this approach and instead introduce a simplifying assumption that ν_t can be replaced with its mean $\bar{\nu}_t$. After deriving analytical solutions for variance swap prices, we can use this assumption to arrive at a lognormal form for the terminal asset value S_T. We can then use the variance swaps and S_T later as effective control variates when estimating the implied volatility skew.

2.3.1 First-order Variance Swaps

We first turn our attention to first-order variance swaps. Variance swaps are derivatives with payoffs that reflect the volatility of its underlying asset. Specifically, its payoff at expiry is given by $\int_0^T \nu_s ds$. We will now use the Heston model to derive a closed form soltion for its current price.

Starting with the variance process SDE in (2.2) we have

$$\nu_t = \nu_0 + \int_0^t \kappa(\theta - \nu_s)\, ds \ + \eta \int_0^t \sqrt{\nu_s}\, dB_s.$$

Taking $\mathbb{Q}$-expectations at time 0 and applying Fubini's Theorem along with the martingale property of Ito integrals yields a deterministic form for the mean of the variance process:

$$\begin{aligned}
\mathbb{E}_0^{\mathbb{Q}}[\nu_t] &= \nu_0 + \mathbb{E}_0^{\mathbb{Q}}\left[\int_0^t \kappa(\theta - \nu_s)\, ds\right] + \mathbb{E}_0^{\mathbb{Q}}\left[\int_0^t \eta\sqrt{\nu_s}\, dB_s\right] \\
&= \nu_0 + \int_0^t \kappa(\theta - \mathbb{E}^{\mathbb{Q}}[\nu_s])\, ds.
\end{aligned}$$

Differentiating with respect to t then gives us a linear ODE in terms of the mean of the variance process:

$$\frac{d\mathbb{E}^{\mathbb{Q}}[\nu_t]}{dt} = \kappa(\theta - \mathbb{E}^{\mathbb{Q}}[\nu_t]), \quad \mathbb{E}^{\mathbb{Q}}[\nu_0] = \nu_0,$$

The solution of this ODE is:

$$\mathbb{E}^{\mathbb{Q}}[\nu_t] = \theta + (\nu_0 - \theta)e^{-\kappa t}. \tag{2.8}$$

Note that this is the mean of the variance process, which we discuss in further detail in the following subsection.

Thus, by the Fundamental Theorem of Asset Pricing and Fubini's Theorem we have that the value of the variance swap at time 0 is

$$\begin{aligned}\mathbb{E}_0^{\mathbb{Q}}\left[\int_0^T \nu_s \, ds\right] &= \int_0^T \mathbb{E}_0^{\mathbb{Q}}[\nu_s] \, ds \\ &= \int_0^T \theta + (\nu_0 - \theta)e^{-\kappa t} \, ds \\ &= \theta T + \frac{1}{\kappa}(\theta - \nu_0)(e^{-\kappa T} - 1). \end{aligned} \tag{2.9}$$

Thus the current value of this variance swap is $\theta T + \frac{1}{\kappa}(\theta - \nu_0)(e^{-\kappa T} - 1)$. This solution can in fact be used to find a closed-form solution for the asset price S_t within the a modified Heston model where ν_t is replaced with $\bar{\nu_t}$. We will see how this is done in the following section.

2.3.2 The Mean-Variance Heston Dynamics

As previously alluded to, we now turn our attention to finding a closed form solution for S_T in the Heston model by replacing ν_t with its mean $\overline{\nu_t}$, as given in equation (2.8). Starting with the risk-neutral dynamics for S_t presented in (2.2) and substituting $\overline{\nu_t} = \mathbb{E}^{\mathbb{Q}}[\nu_t]$ for ν_t we obtain:

$$dS_t = S_t\sqrt{\overline{\nu_t}}dW_t$$

We can then easily obtain the risk-neutral log-dynamics for S_t

$$d\ln S_t = -\frac{1}{2}\overline{\nu_t}dt + \sqrt{\overline{\nu_t}}dW_t$$

We have already obtained the analytical form for the variance swap in (2.9), so the first and second moments of the Gaussian Ito integral can easily be found by the martingale property of Ito integrals and Ito's Isometry, respectively, to yield the lognormal distribution:

$$\ln(\frac{S_T}{S_0}) \overset{d}{=} -\frac{1}{2}\int_0^T \overline{\nu_s}\, ds + \int_0^T \sqrt{\overline{\nu_s}}\, dW_s$$
$$= -\frac{1}{2}\left(\theta T + \frac{1}{\kappa}(\theta-\nu_0)(e^{-\kappa T}-1)\right) + \left(\theta T + \frac{1}{\kappa}(\theta-\nu_0)(e^{-\kappa T}-1)\right)^{\frac{1}{2}} Z$$

where $Z \sim \mathcal{N}(0,1)$, since $\int_0^t \sqrt{\overline{\nu_s}}\, dW_s \sim \mathcal{N}(0, \int_0^t \overline{\nu_s}\, ds)$. Thus it follows that

$$S_T \overset{d}{=} S_0 \exp\left(-\frac{1}{2}\left(\theta T + \frac{1}{\kappa}(\theta-\nu_0)(e^{-\kappa T}-1)\right) + \left(\theta T + \frac{1}{\kappa}(\theta-\nu_0)(e^{-\kappa T}-1)\right)^{\frac{1}{2}} Z\right)$$

This lognormal form provides a convenient analytic expression for the terminal asset price under the Heston model given the substitution of $\bar{\nu_t}$ for ν_t, and a Black-Scholes-like formula can be used to analytically value contingent claims written on S_t. One would naturally be concerned about the appropriateness of this substitution, and directly related to this is the noteworthy absence of η, the volatility of volatility, in the above expression. The substitution effectively "integrates out" the stochasticity of the volatility, making the model more akin to a local volatility model where the volatility varies deterministically with time. Thus, if empirical market data suggests an η near zero and relatively smooth variation in volatility, it would be appropriate, but later in this work we consider (a perhaps unrealistically) high $\eta = 5$ in which case this substitution would likely not be appropriate.

2.3.3 Second-order Variance Swap

We also wish to price a variance claim with payoff dependent on the squared-variance, which would tend to pay more if volatility itself is volatile. The claim has a payoff at time T given by $\int_0^t \nu_s^2\, ds$. First, we apply Ito's product rule to obtain the dynamics of ν_t^2:

$$d\nu_t^2 = 2\nu_t d\nu_t + d\nu_t d\nu_t$$
$$= (\eta^2\nu_t + 2\kappa(\theta-\nu_t)\nu_t)dt + 2\eta\nu_t^{3/2} dB_t$$

Taking expectations, we have

$$\mathbb{E}^{\mathbb{Q}}[\nu_t^2] = \nu_0^2 + (\eta^2 + 2\kappa\theta)\int_0^t \mathbb{E}^{\mathbb{Q}}[\nu_s]\, ds - 2\kappa\int_0^t \mathbb{E}^{\mathbb{Q}}[\nu_s^2]\, ds$$

Differentiating and substituting for $\mathbb{E}^{\mathbb{Q}}[\nu_t]$ from (2.8), this leads us to a linear ODE in $\mathbb{E}^{\mathbb{Q}}[\nu_t^2]$ similar to the one obtained for the first-order variance swap:

$$\frac{d\mathbb{E}^{\mathbb{Q}}[\nu_t^2]}{dt} = (\eta^2 + 2\kappa\theta)\mathbb{E}^{\mathbb{Q}}[\nu_t] - 2\kappa\mathbb{E}^{\mathbb{Q}}[\nu_t^2], \quad \mathbb{E}^{\mathbb{Q}}[\nu_0^2] = \nu_0^2$$
$$= -2\kappa\mathbb{E}^{\mathbb{Q}}[\nu_t^2] + (\eta^2 + 2\kappa\theta)(\theta + (\nu_0-\theta)e^{-\kappa t}), \quad \mathbb{E}^{\mathbb{Q}}[\nu_0^2] = \nu_0^2$$

Multiplying both sides by the integrating factor $e^{2\kappa t}$ and solving the linear ODE gives:

$$\mathbb{E}^{\mathbb{Q}}[\nu_t^2] = \nu_0^2 e^{-2\kappa t} + \frac{1}{\kappa}(\eta^2 + 2\kappa\theta)(\frac{\theta}{2}(1 - e^{-2\kappa t}) + (\nu_0 - \theta)(e^{-\kappa t} - e^{-2\kappa t}))$$

Hence applying Fubini's Theorem and integrating gives the fair price for the second-order variance swap:

$$\mathbb{E}^{\mathbb{Q}}\left[\int_0^T \nu_s^2 \, ds\right] = \frac{\nu_0^2}{2\kappa}(1 - e^{-2\kappa T}) + \frac{1}{2\kappa^2}(\eta^2 + 2\kappa\theta)\left(\frac{\theta}{2}(2\kappa T + e^{-2\kappa T} - 1) + (\nu_0 - \theta)(e^{-2\kappa T}(e^{\kappa T} - 1)^2)\right) \tag{2.10}$$

Now that we have obtained analytical forms for the variance swap prices, we can use them to validate that numerical estimates of the swaps using the discretization schemes lead to the correct results. Furthermore, they can be used as control variates, to decrease Monte Carlo estimation error. In the following chapter we will see how these discretization algorithms and control variates are employed within the Heston model.

Chapter 3

Implementation

In our study of the Heston Model, a primary objective is to estimate the implied volatility skew. In this chapter, we present three discretization methods which allows us to generate sample paths of the volatility and asset price processes, from which we can obtain Monte Carlo estimates of European option prices and obtain the estimated volatility skew. We also discuss the usage and selection of control variates to obtain a variance reduction for the estimated volatility skew.

3.1 Euler-Maruyama Discretization

The first discretization scheme we will consider is the Euler-Maruyama discretization for SDEs, which is an extension of the Euler method for ODEs. The method begins by partitioning the time interval $[0, T]$ into a grid of N increments of size $\Delta t = \frac{T}{N}$: $\{0, \Delta t, 2\Delta t, ..., (N-1)\Delta t, N\Delta t = T\}$. Given an initial value, the SDE can be discretely approximated on this grid by recursively computing consequent values of the process going forward in time. Stochasticity is introduced by generating multivariate normal random variates to approximate the Gaussian Ito increments. The recursive algorithm for the coupled SDE is as follows:

$$\begin{pmatrix} x_{t_k} - x_{t_{k-1}} \\ \nu_{t_k} - \nu_{t_{k-1}} \end{pmatrix} \overset{\mathrm{d}}{=} \begin{pmatrix} -\frac{1}{2}\nu_{t_{k-1}} \\ \kappa(\theta - \nu_{t_{k-1}}) \end{pmatrix} \Delta t + \begin{pmatrix} \sqrt{\nu_{t_{k-1}}\Delta t} Z_k^x \\ \eta\sqrt{\nu_{t_{k-1}}\Delta t} Z_k^\nu \end{pmatrix}$$

where

$$\begin{pmatrix} Z_k^x \\ Z_k^\nu \end{pmatrix} \sim N\left(\begin{pmatrix} 0 \\ 0 \end{pmatrix}, \begin{pmatrix} 1 & \rho \\ \rho & 1 \end{pmatrix} \right)$$

Once multiple sample paths have been generated according to this scheme, the terminal values of the simulated asset price process can be used to compute a Monte Carlo estimate for g as in equation (2.5). One potential problem with this method is that discretization error can cause the volatility process to take on negative values, even though a Feller process cannot take on negative values. This poses a problem in the next iteration when computing the term $\sqrt{\nu_{t_{k-1}}}$; however, this can easily be remedied by substituting $\sqrt{\max(\nu_{t_{k-1}}, 0)}$ for this quantity. Another shortcoming if the Euler Method is that the discretization error will be of order $\mathcal{O}(\sqrt{\Delta t})$, which suggests we may wish to employ a method with a lower discretization error.

3.2 Milstein Discretization

To improve the discretization errors in simulating the SDE, we turn to the Milstein discretization scheme. This method improves on the Euler method by adding a correction term so that the discretization error is now of order $\mathcal{O}(\Delta t)$. This is accomplished by approximating the generic SDE $dy_t = a_t dt + b_t dW_t$ where $a_t = a(y_t)$ and $b_t = b(y_t)$, by:

$$y_{t_k} - y_{t_{k-1}} = a_{t_{k-1}}\Delta t + b_{t_{k-1}}(W_{t_k} - W_{t_{k-1}}) + \frac{1}{2}b(y_t)\partial_y b(y_t)((W_{t_k} - W_{t_{k-1}})^2 - \Delta t) \tag{3.1}$$

Note the first two terms are in fact equivalent to those in the Euler method, while the third term can be referred to as a 'Milstein correction term'. Applying this to our system of SDEs in equation (2.3), we have:

$$\begin{pmatrix} x_{t_k} - x_{t_{k-1}} \\ \nu_{t_k} - \nu_{t_{k-1}} \end{pmatrix} \overset{\mathrm{d}}{=} \begin{pmatrix} -\frac{1}{2}\nu_{t_{k-1}} \\ \kappa(\theta - \nu_{t_{k-1}}) \end{pmatrix} \Delta t + \begin{pmatrix} \sqrt{\nu_{t_{k-1}}\Delta t} Z_k^x \\ \eta\sqrt{\nu_{t_{k-1}}\Delta t} Z_k^\nu \end{pmatrix} + \begin{pmatrix} 0 \\ \frac{1}{4}\eta^2(\Delta t (Z_{k-1}^\nu)^2 - \Delta t) \end{pmatrix}$$

where

$$\begin{pmatrix} Z_k^x \\ Z_k^\nu \end{pmatrix} \sim N\left(\begin{pmatrix} 0 \\ 0 \end{pmatrix}, \begin{pmatrix} 1 & \rho \\ \rho & 1 \end{pmatrix} \right)$$

Note that the Milstein discretization scheme for the asset price process is equivalent to the Euler scheme since x_t does not appear in the Ito term of its SDE. Additionally, discretization error can still result in negative values for $\nu_{t_k - 1}$, so we can instead take $\max(\nu_{t_{k-1}}, 0)$ as in the Euler method. Critically, in cases where this negativity correction is made, the Milstein correction must also be set to zero. This is because the Milstein correction term acts to adjust the Ito term, but if the Ito term is set to zero so must its adjustment. Overall, this scheme results in a lower discretization error on the order $\mathcal{O}(\Delta t)$.

3.3 Mixing Method with Milstein Discetization

To this point, both of the discretization schemes we have explored allowed us to simulate the entire paths of both the volatility and asset price processes. Since we are not evaluating a path-dependent option, it is disadvantageous with respect to computational complexity and error propagation to simulate the entire paths when only the terminal asset price values are required for the Monte Carlo method. Using these methods, the overall error is a combination of simulation error from the discretization schemes and statistical estimation error from the Monte Carlo method. To address this (and hopefully lower the overall error), we turn to a hybrid method referred to as the "Mixing Method," which proceeds as follows.

We can express the option price as an iterated expectation:

$$\mathbb{E}^{\mathbb{Q}}_{t,x,\nu}[G(e^{X_T}, \nu_T)] = \mathbb{E}^{\mathbb{Q}}_{t,x,\nu}[\mathbb{E}^{\mathbb{Q}}_{t,x,\nu}[G(e^{X_T}, \nu_T)|\mathcal{G}]] \tag{3.2}$$

where $\mathcal{G} = \sigma((\nu_s)_{s\in[t,T]})$. Thus when computing the inner expectation, we assume all future paths of ν_t are

known so that within the inner expectation, X_t is normally distributed.

First, to account for the correlation between W_t and B_t we write

$$W_t = \rho B_t + \sqrt{1-\rho^2} B_t^{\perp} \tag{3.3}$$

where $B_t^{\perp}$ is independent of B_t.

Substituting (3.3) into the integral form of the SDE for X_t in (2.3) we obtain:

$$X_T = X_t - \frac{1}{2}\int_t^T \nu_u du + \int_t^T \sqrt{\nu_u}\rho dB_u + \int_t^T \sqrt{\nu_u(1-\rho^2)} dB_u^{\perp} \tag{3.4}$$

Note that B_t is measurable with respect to $\mathcal{G}$, and so the only random component in (3.4) is $B_t^{\perp}$. Therefore, X_T has a conditional distribution of the following form:

$$X_T|\mathcal{G} \overset{\mathrm{d}}{=} A + \sqrt{B} Z^{\perp}, \qquad Z^{\perp} \overset{\mathbb{Q}}{\sim} N(0,1) \tag{3.5}$$

where

$$A = X_t - \frac{1}{2}\int_t^T \nu_u du + \int_t^T \sqrt{\nu_u}\rho dB_u \tag{3.6}$$

$$B = \mathbb{V}^{\mathbb{Q}}\left[\int_t^T \sqrt{\nu_u(1-\rho^2)} dB_u^{\perp} \;\middle|\; \mathcal{G}\right] = (1-\rho^2)\int_t^T \nu_u du \tag{3.7}$$

The method then proceeds as follows. The first step is to simulate paths of ν_t (but not X_t) using the Milstein method as before. Next, we compute A and B given the simulated paths of ν_t. While the two integrals in A and B do not have closed form solutions, they can very easily be computed numerically via standard summation methods. The key is to re-use the same random variates used to generate ν_t when computing the measurable Ito integral in (3.6). One must then observe the Black-Scholes like form of the conditional distribution of X_T in (3.5). We can relate $A = (r_{BS} - \frac{1}{2}\sigma_{BS}^2)T$ and $B = \sigma_{BS}^2 T$ where $r_{BS}, \sigma_{BS} \geq 0$, we can now write (3.5) as:

$$X_t|\mathcal{G} \overset{\mathrm{d}}{=} (r_{BS} - \frac{1}{2}\sigma_{BS}^2)T + \sigma_{BS}^2 T Z^{\perp}$$

We can then solve for the implied Black-Scholes parameters:

$$\sigma_{BS} = \sqrt{\frac{B}{T}} \qquad r_{BS} = \frac{A}{T} + \frac{B}{2T}$$

We can then simply the conditional future value of the option price (the inner expectation in (3.2)) in closed form using the Black Scholes formula with the implied parameters:

$$g_t = e^{r_{BS}t} V^{BS}(K, T, t, S_0, r_{BS}, \sigma_{BS})$$

Next, we can compute the outer expectation numerically by averaging (across the simulations of ν_t) the option prices determined in closed form. Lastly, the Black-Scholes formula can be inverted as before to obtain the implied volatility smirk using the true parameter $r = 0$. The advantage of this method over the previous two is that rather than computing both expectations numerically, the conditioning allows the inner expectation to be computed analytically and only the outer expectation must be computed numerically. In addition, we no longer need to simulate the entire path of the asset price process, resulting in a quicker estimation of the implied volatility smirk.

3.4 Control Variates

The control variates technique is a method to reduce the variance of a Monte Carlo estimate of X. Suppose we have N control variates $Y^{(1)}, Y^{(2)}, ..., Y^{(N)}$, which form the vector $\boldsymbol{Y}$ with known (or easily computable) mean $\boldsymbol{h}$. Construct the quantity

$$W = X + \boldsymbol{\gamma}^T(\boldsymbol{h} - \boldsymbol{Y})$$

Clearly, $\mathbb{E}[W] = \mathbb{E}[X]$, which is equivalent to the standard monte carlo estimate. Let $\boldsymbol{\Sigma_{YY}}$ be the covariance matrix of Y_i and $\boldsymbol{\Sigma_{XY}}$ be the vector whose elements are the covariances between Y_i and X. The variance of W is then:

$$Var(W) = Var(X) + \boldsymbol{\gamma}^T\boldsymbol{\Sigma_{YY}}\boldsymbol{\gamma} - 2\boldsymbol{\gamma}^T\boldsymbol{\Sigma_{XY}}$$

Which is minimized at

$$\hat{\boldsymbol{\gamma}} = (\boldsymbol{\Sigma_{YY}})^{-1}\boldsymbol{\Sigma_{XY}}$$

Substituting the optimal γ into $Var(W)$ yields:

$$Var(W) = (1 - R^2_{\boldsymbol{XY}})Var(X)$$

Where $R^2_{\boldsymbol{XY}} = \boldsymbol{\Sigma_{XY}}^T(\boldsymbol{\Sigma_{YY}})^{-1}\boldsymbol{\Sigma_{XY}}/Var(X)$ is the squared multiple correlation coefficient between X and $\boldsymbol{Y}$. A strong choice of control variates leading to an efficient variance reduction is therefore to choose a set of control variates which are highly correlated (in magnitude) with X, while trying to maximize orthogonality between the control variates themselves.

In the context of estimating an implied volatility smirk, X are simulated option payoffs, and we seek a variance reduction for the Monte Carlo estimates of the option price to reduce the confidence bands for the option price and consequently the implied volatility smirk. Hence, $X = G(S_T, K, T) = (S_T - K)_+$ or

$X = G(S_T, K, T) = (K - S_T)_+$ for calls and puts respectively.

Our first choice of control variate is the exact same option payoff $G(S_T)$ that we are computing a Monte Carlo estimate of, where we introduce the simplifying asssumption of replacing ν_t with $\bar{\nu}_t$. Our second choice of control variate is the termianl asset value itself, S_T. These should be strong correlated with the option payoff, making them effective control variates. Of course, we must be able to compute their means easily, which we can easily do since our simplifying assumption gives us a lognormal form for S_T described in (2.3.2). We must obtain $\mathbb{E}^{\mathbb{Q}}[S_T]$ and $\mathbb{E}^{\mathbb{Q}}[G(S_T)]$. To find these closed forms we first set the variance swap price

$$\mathbb{E}^{\mathbb{Q}}\left[\int_0^T \nu_s ds\right] = \int_0^T \overline{\nu_s} ds = \theta T + \frac{1}{K}(\theta - \nu_0)(e^{-\kappa T} - 1) := \alpha$$

Then by 2.3.2, we have the following

$$S_T = S_0 e^{\frac{1}{2}\alpha + \sqrt{\alpha} Z}$$

where $Z \sim N(0, 1)$.

Now we can find $\mathbb{E}^{\mathbb{Q}}[S_T]$ using the moment generation function for the standard normal as follows:

$$\mathbb{E}^{\mathbb{Q}}[S_T] = S_0 \mathbb{E}^{\mathbb{Q}}[e^{\frac{1}{2}\alpha + \sqrt{\alpha} Z}] = S_0 e^{-\frac{1}{2}\alpha + \frac{1}{2}\alpha} = S_0$$

Furthermore, notice that S_T in equation 3.4 is in the form of a geometric brownian motion. Therefore, $\mathbb{E}^{\mathbb{Q}}[G(S_T)]$ is simply the Black-Scholes option price with volatility α.

The last two control variates we will use are the first and second order varianace swaps, as we hypothesize that if ρ in the Heston model is not near zero they may be correlated positively or negatively with the option price leading to a variance reduction. We have already found closed forms for their expectation under $\mathbb{Q}$ in equations 2.9 and 2.10.

To summarize, we will use the following control variates:

$$\boldsymbol{Y} = \begin{pmatrix} G(S_T) \\ S_T \\ \int_0^T \nu_s ds \\ \int_0^T \nu_s^2 ds \end{pmatrix} \tag{3.8}$$

which can be approximated by the m'th simulated values as follows:

$$\boldsymbol{Y^{(m)}} = \begin{pmatrix} G(S_T^{(m)}) \\ S_T^{(m)} \\ \sum_{k=0}^N \nu_{t_k}^{(m)} \Delta t \\ \sum_{k=0}^N (\nu_{t_k}^{(m)})^2 \Delta t \end{pmatrix} \tag{3.9}$$

Furthermore, using the aforementioned results from chapter 2, we have the following closed-form expectations for the control variates:

$$\boldsymbol{h} = \begin{pmatrix} V^{BS}(K,T,S_0,r,\sigma=\alpha) \\ S_0 \\ \alpha \\ \frac{\nu_0^2}{2\kappa}(1-e^{-2\kappa T}) + \frac{1}{2\kappa^2}(\eta^2+2\kappa\theta)\left(\frac{\theta}{2}(2\kappa T + e^{-2\kappa T}-1) + (\nu_0-\theta)(e^{-2\kappa T}(e^{\kappa T}-1)^2)\right) \end{pmatrix} \tag{3.10}$$

The rest of the control variate implementation follows quite quickly, as we can easily obtain numerical sample estimates for $\boldsymbol{\Sigma_{YY}}$ and $\boldsymbol{\Sigma_{XY}}$, which can then be used to solve for γ.

In the next chapter, we will explore the resulting volatility smiles that are obtained by implementing the aforementioned estimation techniques.

Chapter 4

Results and Discussion

4.1 Estimating the Volatility Smirk

In this section, we implement the simulation techniques discussed in previous sections for the base set of Heston model parameters:

$$\{r = 0, S_0 = 1, \sqrt{v_0} = 30\%, \kappa = 3, \sqrt{\theta} = 40\%, \eta = 5, \rho = -0.5\}$$

We will use this base set of parameters for the bulk of the implied volatility smile simulations to maintain consistency, and then explore the effect of changing these parameters separately on the smile separately. First, we generate sample paths of the coupled volatility and asset price process using the Euler discretization method. Twenty simulated paths of the coupled process can be seen in figure 4.1.

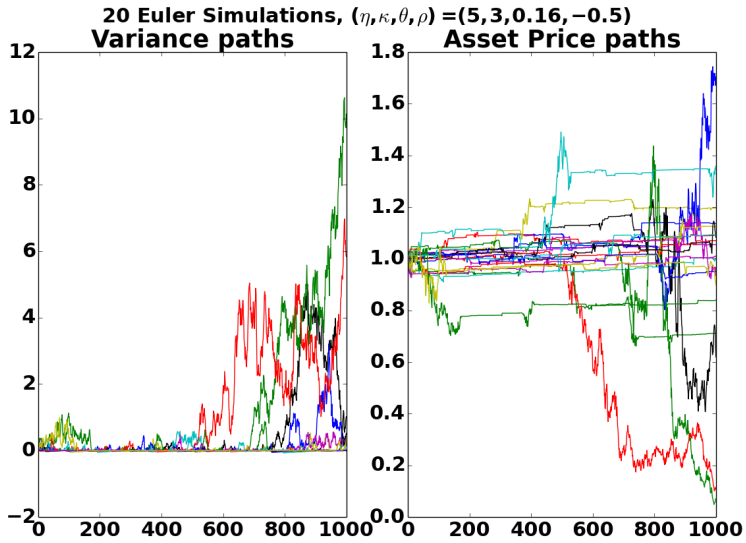

Figure 4.1: 20 sample variance and asset price paths using the Euler discretization method.

An interesting observation regarding the simulated paths is that most of the volatility process tend to zero, and then very large shocks occur. The corresponding behavior of the asset prices is that when the volatility is near zero, the asset price doesn't move much, and then when a large shock arrives the asset price becomes very volatile. This is attributed to the choice of $\eta = 5$, which is very large and likely not appropriate to model most liquid traded assets. The large volatility of volatility causes the volatility to shrink to zero, and then gets stuck there due to the $\sqrt{\nu_t}$ term in the Feller Process. Similarly, once it drifts far enough from zero, another large shock can arrive due to the large η and cause a large jump in volatility and thus a large jump in the asset price. A choice of large η may be appropriate for certain sparsely-traded assets with poor liquidity, which have little short-term volatility. However, on the arrival of substantial news, disproportionately large shocks can arrive, similar to the simulated asset prices in 4.1.

Another important observation regarding the simulated paths is that large positive jumps in volatility correspond to large negative jumps in the asset price, and vice versa. This is attributed to the choice of negative $\rho = -0.5$, which enables the Heston Model to capture the volatility skew.

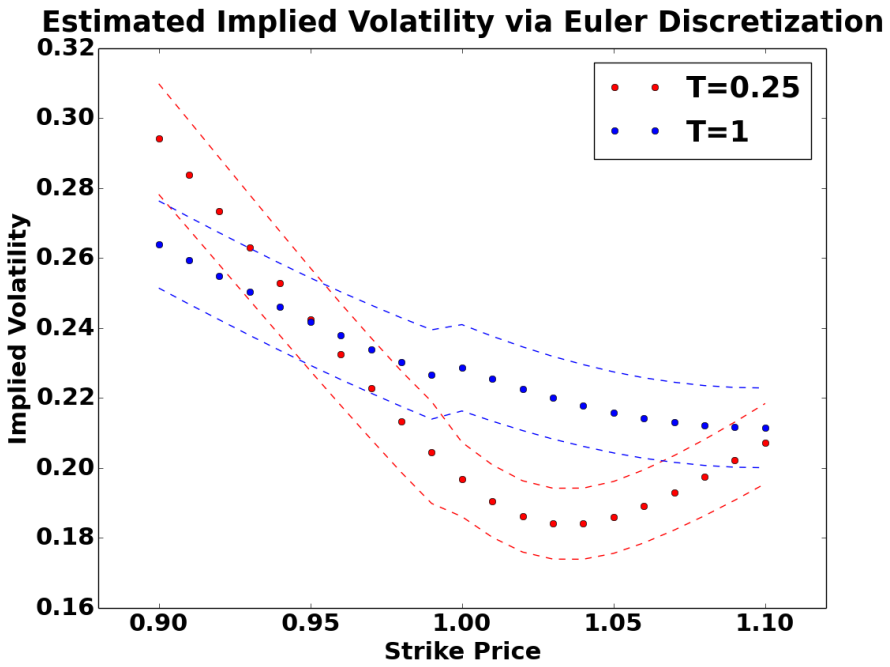

Figure 4.2: Estimated implied volatility smiles with 95% confidence bands using Euler discretization method, plotted with respect to the strike price K.

Next, we are interested in examining the estimated volatility smirk from the Monte-Carlo estimated option prices where the volatility and asset price are simulated using the Euler method. The estimated smiles - two

slices of the volatility surface - for options of maturity $T = 0.25$ and $T = 1$ years are shown in Figure 4.2, together with the corresponding 95% confidence bands from the Monte Carlo standard error.
The first noticeable observation regarding the estimated volatility skew is that it is is skewed to the left with higher implied volatility for lower strikes, which is characters tic of the empirical volatility skew for equity options. This can be directly explained by the choice of negative correlation $\rho = -0.5$. Since ν_t is bounded below by zero but not bounded from above, it can take larger jumps upwards, and the negative correlation associates large upwards jumps in volatility with large downwards jumps in the asset price. Since large downside jumps become more likely than in the constant volatility case, options with lower strikes tend to be priced higher, meaning they have higher implied volatilities. If ρ is instead positive, these unbounded large jumps in volatility correlate with large upwards jumps in asset price, causing the volatility smirk to be skewed to the right (higher for larger strikes).

Another critical observation about the estimated volatility smirk in Figure 4.2 is how the smirk is flatter for larger $T = 1$. In fact, this holds generally for the Heston Model. As T tends to infinity, the volatility surface tends to a flat plane. This is an attribute of the mean-reverting nature of the Feller Process. With little time to expiration, there is a higher chance that the volatility at settlement will be near a "current" value of the volatility process which may be distant from the long-run mean θ. However, with more time, there is a higher likelihood that the volatility process will revert to its mean, suggesting that the "fair smirk" is a flat line.

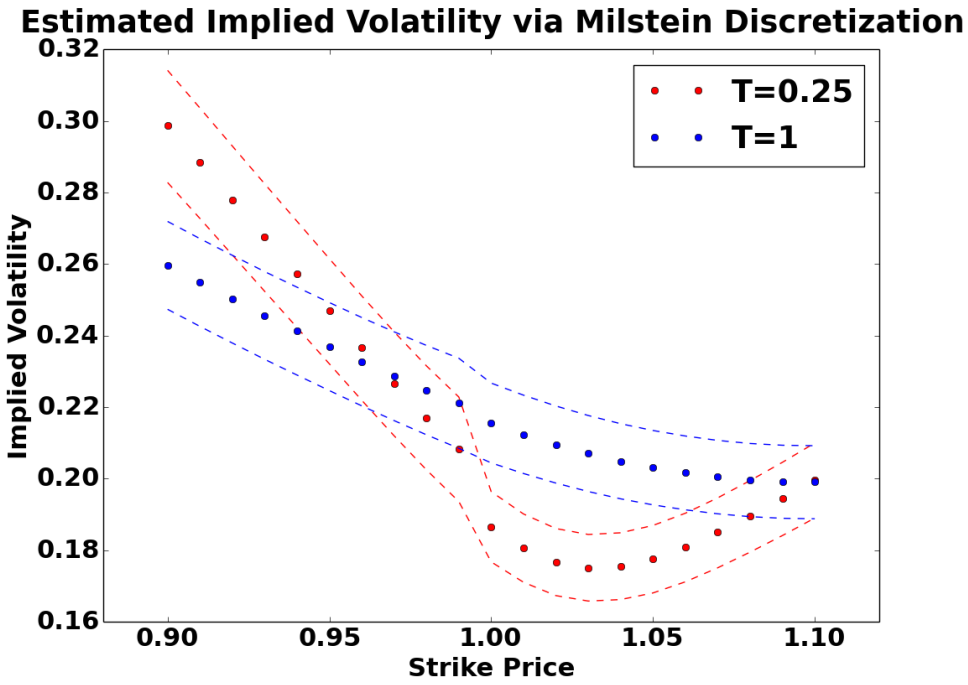

Figure 4.3: Estimated implied volatility smiles with 95% confidence bands using Milstein discretization method

We also examine the same estimated volatility smirks using the Milstein discretization method, shown in Figure 4.3. There is not a tremendous difference between the Euler and Milstein estimates, although the confidence bands may be slightly narrower in the Milstein estimates due to the added correction term. In both Euler and Milstein methods, there is a slight kink in the smirks at $K = 1$. This is due to the use of out-of-the money options and thus a swap between the use of puts for strikes $K < 1$ and calls for strikes $K \geq 1$. Although put-call parity would imply a unique implied volatility for a put and call with the same strike price, observe that we are replacing analytical option prices with Monte Carlo estimates of the option prices, which have some associated error. Hence, put-parity only holds approximately for the simulated option prices, resulting in slight simulation differences between call and put-derived implied volatilities.

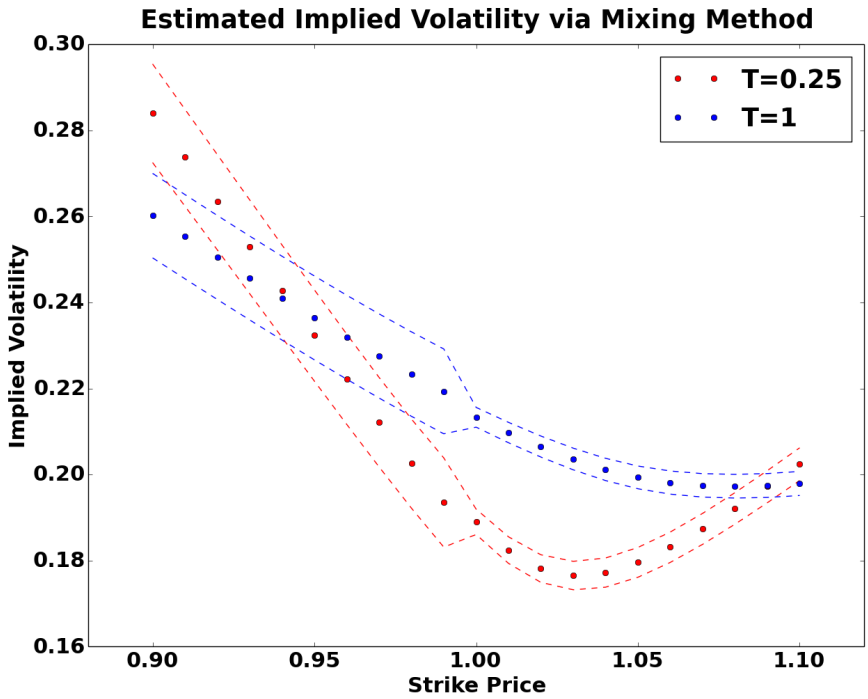

Figure 4.4: Estimated implied volatility smiles with 95% confidence bands using the Mixing method.

Next, we estimate the implied volatility smirks with the mixing method, which leverages iterated expectations to reduce the estimation error by computing the inner expectation analytically. The estimated smirks can be seen in Figure 4.4. Perplexingly, we obtain an as-desired variance reduction for calls, but a negligible variance reduction for puts. While we struggled to arrive at a comprehensive explanation for this phenomenon, we observed that this variance asymmetry gets reversed when ρ is positive. That is, when ρ is positive, not only does the skew go to the right, but the variance reduction occurs for puts and not for calls. We also found that when $\rho = 0$, the variance asymmetry between calls and puts disappears. This can be seen in Figures 6.12 and 6.13 in the Appendix. Thus, we posit that negative correlation causes larger adverse events on the downside for the asset price when volatility spikes, and thus larger Monte Carlo standard error for puts, and vice versa when correlation is positive.

4.2 Implied Volatility Smirk Variance Reduction through Control Variates

Next we look to improve our estimate for the volatility smiles using the control variates given in equation (3.8). We first implement the control variates variance reduction using a Milstein discretization scheme with the resulting volatility smirk given in Figure 4.5. It is apparent that the use of control variates reduced the size of our confidence bands in comparison to those plotted in Figure 4.3. This is expected, as control variates are specifically selected to be correlated with the option prices and employed to reduce the standard error of the Monte Carlo approximation. Thus, it appears to have validated our guess that the control variates had an adequate amount of correlation with the option price in order to significantly reduce the size of the confidence band.

Another noteworthy improvement in Figure 4.5 in contrast to 4.3 is the elimination of the kink in the smirk at strike price $K = S_0 = 1$. As mentioned in the previous section, the kink in Figure 4.3 can be attributed to the Monte Carlo estimated option prices not perfectly satisfying put-call parity. By reducing the variability of the Monte Carlo estimate, we have also reduced the magnitude of the violation of put-call parity, leading to a reduction in this kink.

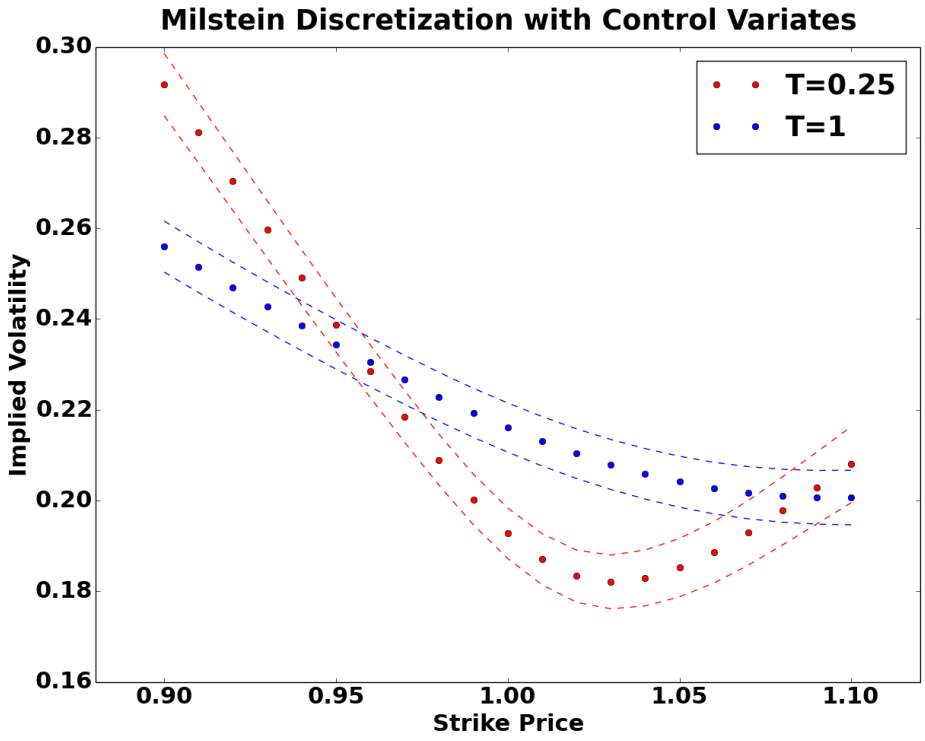

Figure 4.5: Estimated implied volatility smiles with 95% confidence bands using the Milstein scheme and control variates.

We now turn our attention to the plot produced when using the mixing method with control variates in Figure 4.6. Similar to the Milstein method, the dramatic tightening of the confidence intervals in comparison to those in figure 4.4 is due to the reduction in the Monte Carlo standard error as a result of introducing the control variates. Since there is only one expectation approximated via Monte Carlo for the Mixing Method, it is consistent with expectations to have narrower confidence bands than the Milstein Method featured. In addition, the ρ-dependent assymetry in standard error between calls and puts seen in Figure 4.4 has been eliminated by introducing control variates.

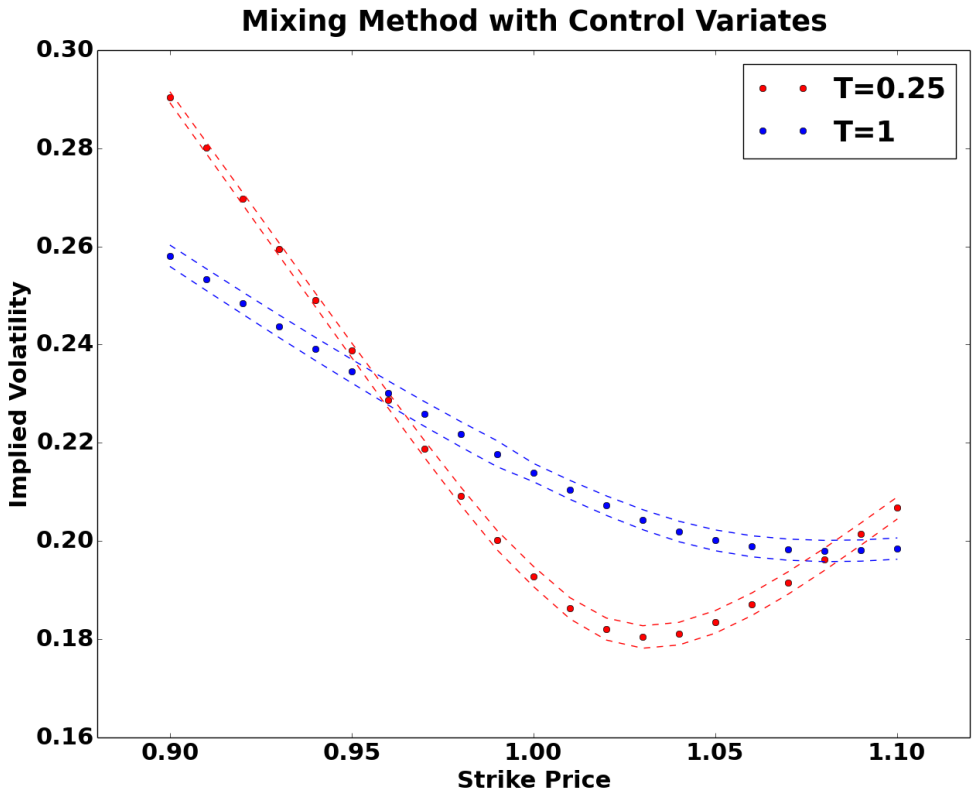

Figure 4.6: Estimated implied volatility smiles with 95% confidence bands using the Mixing method and control variates.

To summarize, both figures 4.5 and 4.6 exemplify a visible reduction in size of the confidence band and hence a significant reduction in Monte Carlo standard error due to the addition of the control variates.

4.3 The Effect of the Heston Parameters on the Implied Volatility Skew

In Figures 6.1-6.6 of the Appendix, 20 sample paths of the volatility and asset price processes using the Milstein discretization scheme are shown for various Heston Model parameters. Similarly, in Figures 6.7-

6.11, the estimated volatility skews for comparable Heston model parameters are shown, once again using thte Milstein method. Based on these results, the behaviour of the Heston Model Parameters can be summarized in the following manner:

- κ: The mean-reverting rate of the Feller Process. Higher values of κ cause the volatility process to revert from very large or small values, which causes the asset-price process to be less likely to stay flat or be highly volatile. Increasing κ flattens the volatility smirk.
- θ: The long-run mean of the Feller Process. Higher values of θ cause average volatility to increase, which leads to more volatile asset prices. Increasing θ causes an upwards shift in the volatility smirk.
- η: The volatility of the volatility. Higher values of η cause larger shocks in volatility, which can also cause volatility to get "stuck" near zero sometimes. Increasing η increases the convexity of the volatility smirk.
- ρ: The correlation between volatility and asset prices. Positive values of ρ cause large spikes in volatility to associate with large positive jumps in asset price, while negative values of ρ cause large spikes in volatility to associate with large negative jumps in asset price. Positive values of ρ cause the volatility smirk to be right-skewed (higher for larger strikes), negative values of ρ cause the volatility smirk to be left-skewed (higher for lower strikes), and $\rho = 0$ results in a symmetric volatility smile.

4.4 The volatility mean and pricing variance swaps

Here we examine and compare some of the quantities we were able to estimate analytically from the Heston model to their simulated counterparts. Recall that we found a closed form for the mean of the variance process in equation 2.8. In figure 4.8, we compare this analytically computed mean of ν_t ($\overline{\nu_t}$) with one Milstein simulated run of the variance process ν_t. In figure 4.9, we use the simulated variance path to obtain one run of the Milstein simulated asset price path, which we plot with an asset price path using $\overline{\nu_t}$ as the variance (as seen in equation 2.3.2). Also, in figure 4.4, we plot $\overline{\nu_t}$ with the Monte Carlo estimation of the mean of ν_t computed over M Milstein simulations.

These plots allow us to examine several characteristics of our estimation technique and the Heston Model itself. To begin, $\overline{\nu_t}$ is a smooth curve when plotted with respect to time, as seen in blue in figures 4.4 and 4.8. Meaning the volatility itself is now longer stochastic and is dependent only on time, as mentioned previously this is somewhat similar to a local volatility model. On the other hand, in figure 4.8 we see that a single run of stochastic ν_t either hovers around 0 or spikes up massively and quickly. The hovering around 0 is due to the fact that we have to take the maximum of ν_t and 0 at each time step in our discretization scheme in order to assure we are not taking a negative square-root. Hence, due to the high vol-vol of $\eta = 5$ the volatility process varies a great deal but gets caught at 0 sometimes. This explain why ν_t in figure 4.8 is seemingly flat over certain periods of time, while extremely sharp at others. Furthermore, as we can see in figure 4.9, this causes the corresponding asset price path (in green) to exhibit similar behaviour of being quite flat at certain points in time, but extremely volatile at others. Comparatively, the simulated asset price path in blue varies far more consistently, which makes sense since its corresponding volatility is $\overline{\nu_t}$, which varies only

deterministically with time.

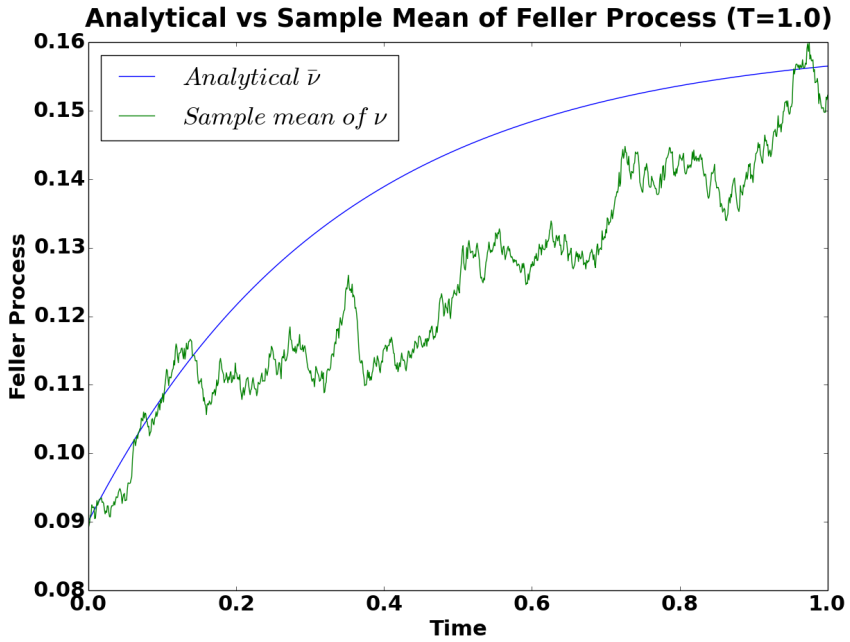

Figure 4.7: The simulated volatility process mean and the mean of ν_t ($\overline{\nu_t}$) plotted with respect to time.

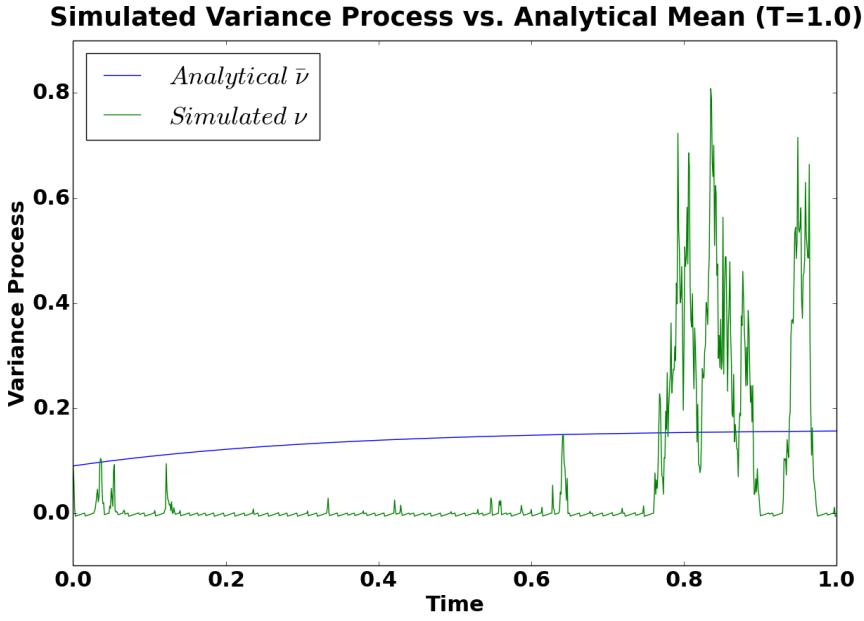

Figure 4.8: One run of the volatility process and the mean of ν_t, $\overline{\nu_t}$ plotted with respect to time.

In figure 4.8, the single run of the volatility process seems to behave quite differently to its analytical mean. However, in figure 4.4, the Monte Carlo mean of the simulated ν_t paths seem to somewhat converge to its analytical mean. This is to be expected since, as previously stated, with a vol-vol of $\eta = 5$, ν_t is a rather volatile stochastic process. Hence a single run of the volatility path is unlikely to exhbit similar behaviour to its analytical mean, but the average of these paths *somewhat* will. We emphasize somewhat since the simulated mean still tends to be less than its analytic counterpart.

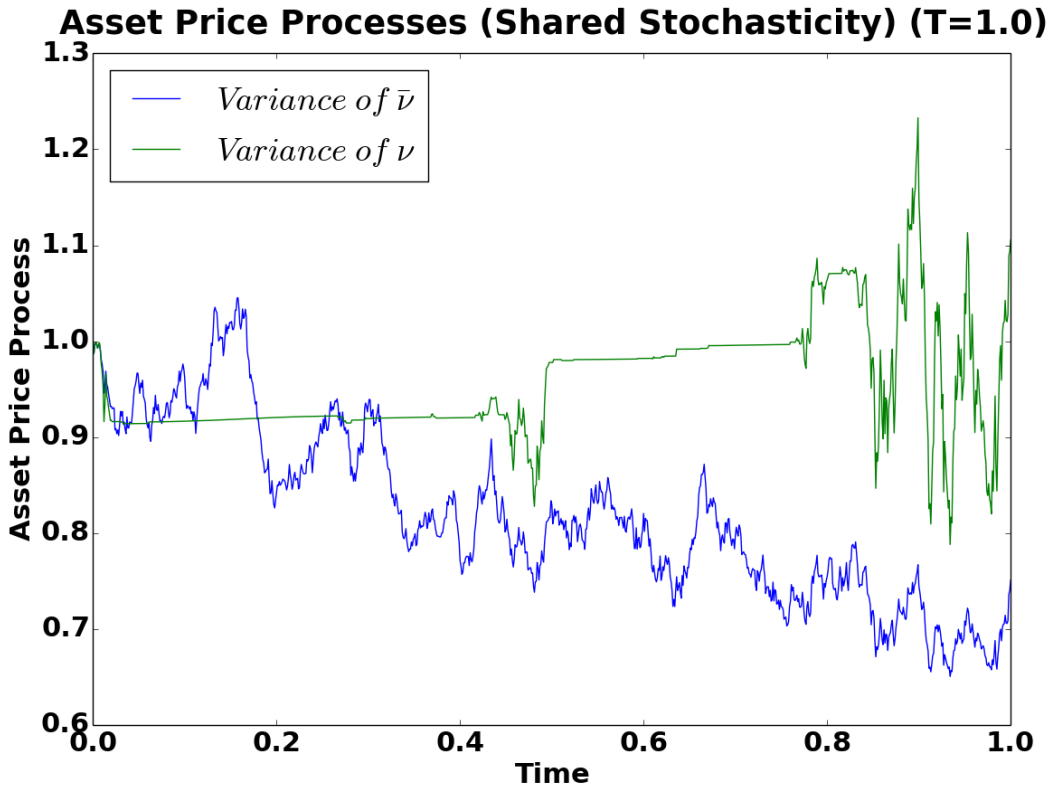

Figure 4.9: One run of the asset price process and the analytical asset price found by substituting $\overline{\nu_t}$ for ν_t plotted with respect to time.

It is difficult to assess whether this model gives an accurate picture of the market, as that depends entirely on the underlying asset at play. The Feller process simulation using the parameters we selected reflects the behaviour of an asset whose volatility is changing rapidly and randomly at some points in time and is stuck close to 0 at other points in time. Furthermore, the points in time at which its highly volatile and not volatile are random as well. In sum, we would use this model with these model parameters to examine an asset that exhibits unpredictable volatility.

The other quantities we were able to estimate analytically were the values of variance swaps. In table 4.1 and 4.2, we computed the analytical values of the first and second order variance swaps, as given in equations 2.9 and 2.10, respectively. We then also estimated these quantities using simulated values, as

described in the last two entries of the matrix 3.9, and taking the Monte Carlo mean. We also compute the relative error between the true and simulated values, which is given by:

$$\epsilon = \frac{|y - y_{approx}|}{y}$$

where y is the analytical value of the swap and y_{approx} is its Monte Carlo estimate using simulated values.

T	0.1	0.2	0.3	0.4	0.5	0.6	0.7	0.8	0.9	1
Analytical Result	0.0100	0.0215	0.0342	0.0477	0.0619	0.0765	0.0915	0.1068	0.1222	0.1378
Estimate	0.0100	0.0214	0.0335	0.0478	0.0614	0.0767	0.0917	0.1061	0.1219	0.1360
Relative Error	0.0047	0.0025	0.0191	0.0023	0.0070	0.0020	0.0022	0.0066	0.0028	0.0131

Table 4.1: First-order variance swap analytical value, estimated value and their absolute difference for different expiry times T.

T	0.1	0.2	0.3	0.4	0.5	0.6	0.7	0.8	0.9	1
Analytical Result	0.0110	0.0382	0.0769	0.1239	0.1769	0.2341	0.2945	0.3573	0.4217	0.4874
Estimate	0.0114	0.0384	0.0784	0.1275	0.1848	0.2211	0.2866	0.3582	0.4166	0.4915
Relative Error	0.0355	0.0044	0.0188	0.0289	0.0452	0.0554	0.0268	0.0027	0.0122	0.0084

Table 4.2: Second-order variance swap analytical value, estimated value and their absolute difference for different expiry times T.

To interpret the data in Table 4.1 and Table 4.2 it will be easiest to examine what a variance swap is in an intuitive sense. One can think of the payoff function $\int_0^T \nu_s \, ds$ as the amount of realized volatility experienced by the underlying from time 0 to time T. In order to value it, we take its mean at time 0. With this in mind, it makes sense that on a longer time horizon the underlying asset will experience more volatility on average, so the fair price of the swap is higher. This is exemplified by the increases in price in 4.1 as T gets larger. Next, notice that the fair values for the second order variance swaps are much higher (Table 4.2). The reason for this comes from the behavior squared integrals. Namely, that values of $|\nu|$ that are greater than 1 are accentuated in the value of the integral. Since $\eta = 5$, the probability that this occurs is higher (and more so on a longer time horizon). Thus the fair price of the second order swap is higher than that of the first order swap.

In the next chapter we will summarize our analysis from this section, as well as give some overarching remarks about stochastic volatility models as a whole, and how they relate to the models we have studied in previous projects.

Chapter 5

Conclusions

We have now explored several characteristics, estimation techniques and financial instrument pricing methods related to the Heston model. The lack of a simple closed form solution for the asset price and volatility (as in Black-Scholes) in this stochastic volatility model offers several challenges in estimation and computation. As with any problem that requires employing approximation techniques, we are faced with both the issue of accurately estimating the quantity at hand and the challenge of minimizing estimation error. After employing a host of techniques, we found that when using a mixture model with the control variates given in equation 3.8 yields an estimate for the implied volatility with a small standard error.

Although this model comes with the potential for estimates with high errors when estimating option prices, it still offers many advantages when compared to the Black-Scholes model, which employs a volatility parameter that is constant through time. As we have discussed earlier, this does not reflect reality as volatility measures the uncertainty associated with an asset's value, which varies constantly with time. Even in comparing our stochastic volatility Heston model to its counterpart resulting from replacing ν_t with its mean. The volatility in this case varies through time, but it does so deterministically, not randomly. This offers a Black-Scholes-like closed-form solution for the option price, but it comes with the caveat of removing the stochasticity from the volatility process.

In addition to addressing one of the critical shortcomings of the Black-Scholes model, the Heston Model also offers an additional opportunity to customize volatility to best suit the behaviour we would expect from the asset. In the appendix we explore how the volatility smiles and the simulated asset price and volatility paths behave when using different parameters. We have discussed throughout this project that the selection of a vol-vol of $\eta = 5$ is quite high and leads to random combination of large spikes and volatility and the volatility getting stuck at 0. The trapping of ν_t at 0 is also due in part to the discretization error causing ν_t at times to dip below 0, which we then take to be 0 by taking the maximum of ν_t and 0 at each iteration. A problem like this needs to kept in mind when choosing model parameters, as simulation errors need to be addressed. On this note, an additional challenge of the model and extension of the project is selecting appropriate parameters for a specific asset whose implied volatility (or associated option prices) we are interested in computing. A Bayesian-based parameter selection process might be interesting to explore,

as this would allow us to incorporate our prior knowledge and current stock data into model parameters. Another approach is to have the model parameters vary through time or be stochastic themselves. The latter approach may involve additional approximation schemes however, and may therefore add sources of error.

The challenges of employing a stochastic volatility model are apparent, but the advantage of being able to customize a volatility process to best suit the asset of interest arguably outweighs the disadvantages in many scenarios. This is especially the case when we are able to decrease the simulation and estimation errors by using analytic results to decrease the amount of approximation required. This tactic of combining closed form solutions within the model with numerical approximations and Monte Carlo estimation leads to better estimation than either simplifying the model to obtain a fully analytic solution or just throwing as many approximation algorithms as we can at the model. This middle ground approach can be applied beyond the Heston model and beyond finance in general.

Chapter 6

Appendix

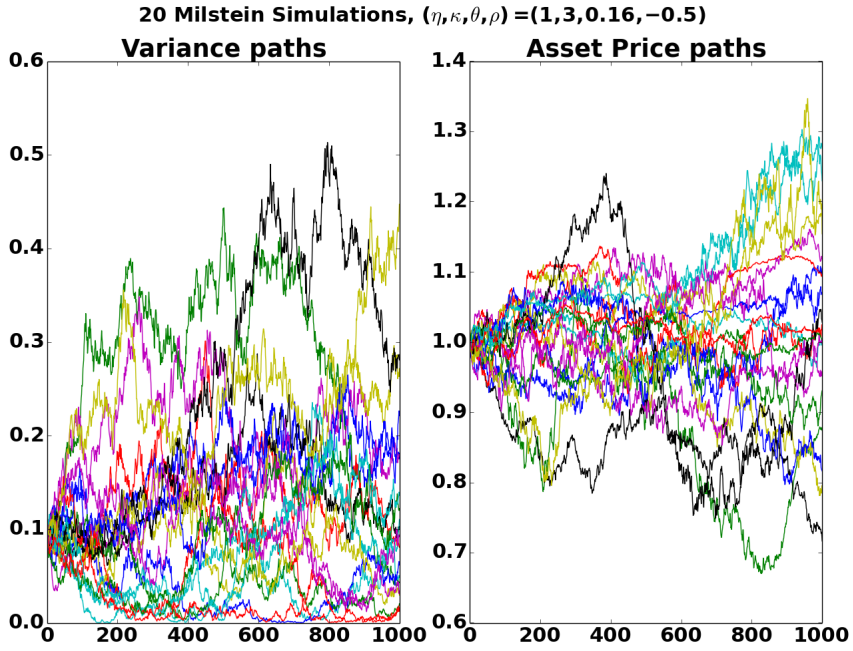

Figure 6.1: Twenty Milstein variance and asset price paths with $(\eta, \kappa, \theta, \rho) = (1, 3, 0.16, -0.5)$.

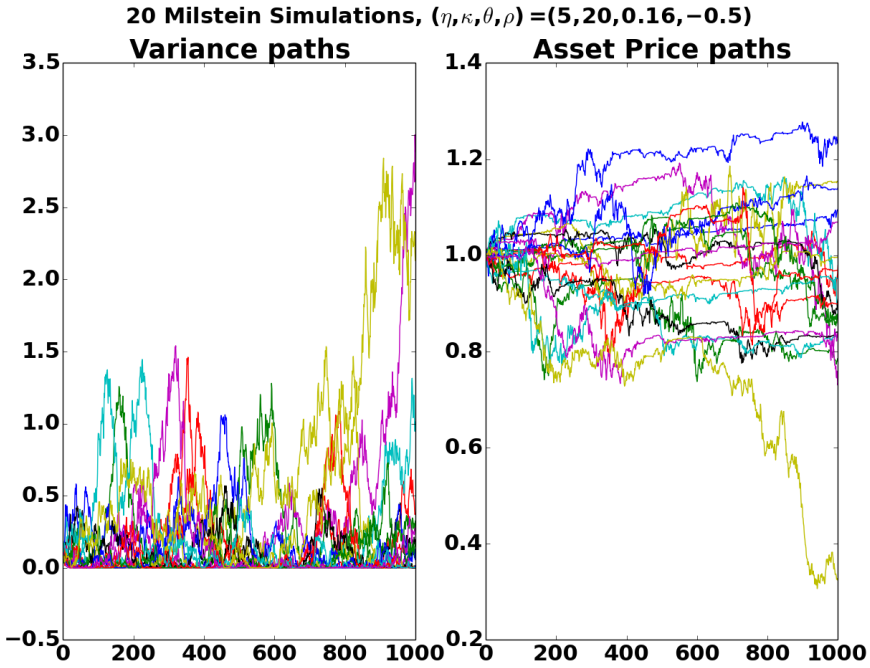

Figure 6.2: Twenty Milstein variance and asset price paths with $(\eta, \kappa, \theta, \rho) = (5, 20, 4, -0.5)$.

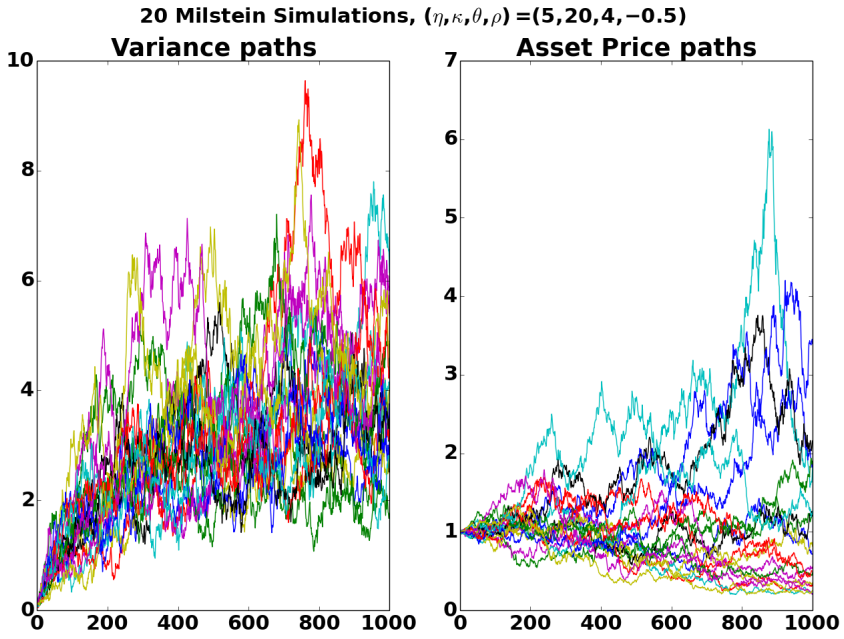

Figure 6.3: Twenty Milstein variance and asset price paths with $(\eta, \kappa, \theta, \rho) = (5, 20, 0.16, -0.5)$.

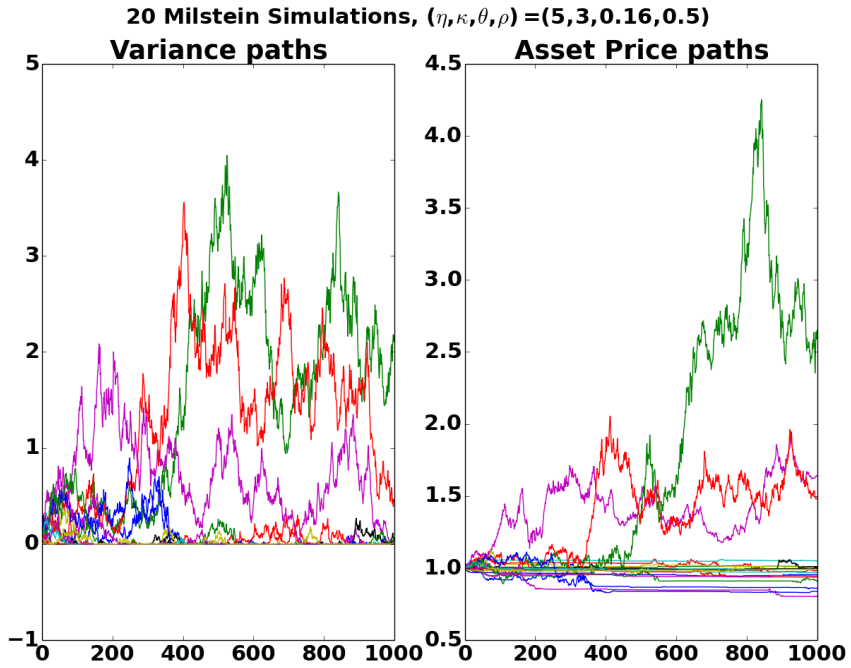

Figure 6.4: Twenty Milstein variance and asset price paths with $(\eta, \kappa, \theta, \rho) = (5, 20, 4, -0.5)$.

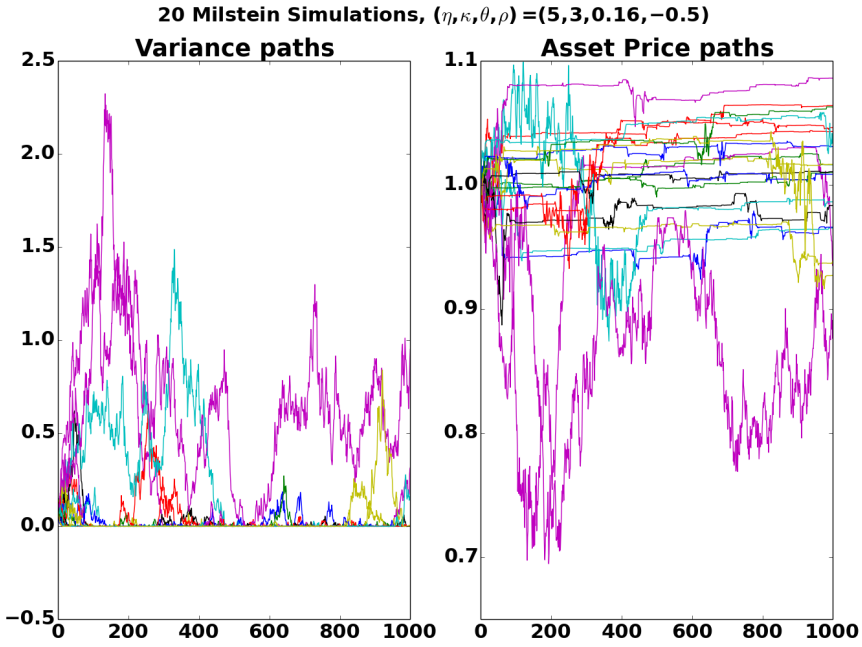

Figure 6.5: Twenty Milstein variance and asset price paths with $(\eta, \kappa, \theta, \rho) = (5, 3, 0.16, 0.5)$.

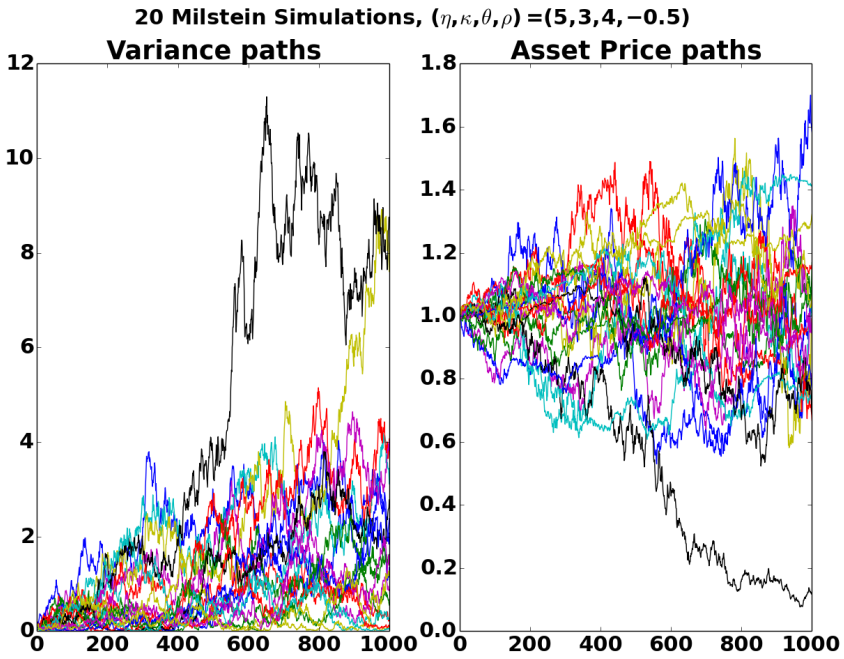

Figure 6.6: Twenty Milstein variance and asset price paths with $(\eta, \kappa, \theta, \rho) = (5, 3, 4, -0.5)$.

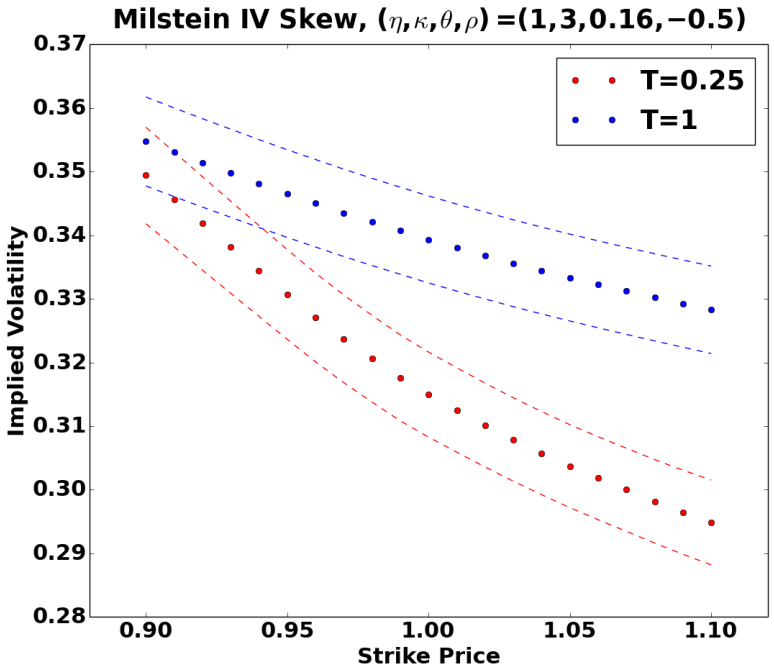

Figure 6.7: Twenty Milstein variance and asset price paths with $(\eta, \kappa, \theta, \rho) = (1, 3, 0.16, -0.5)$.

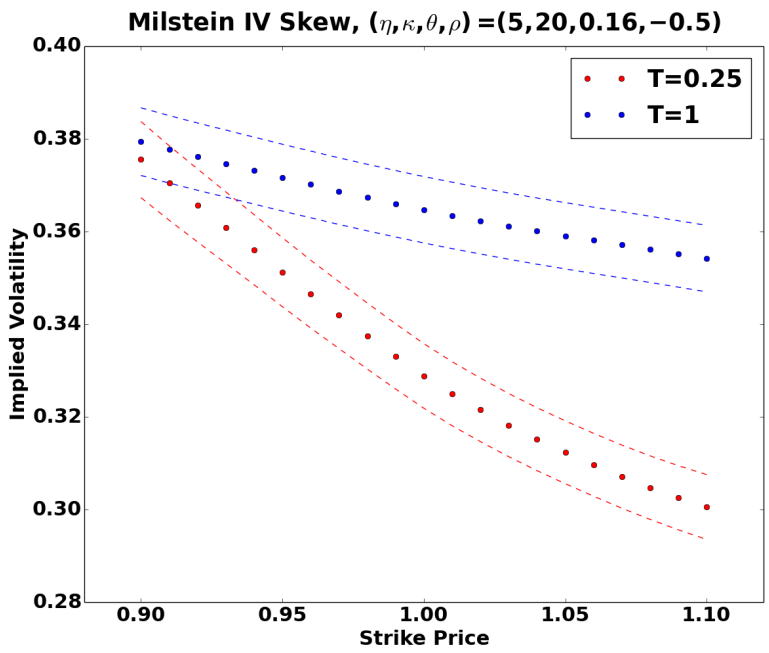

Figure 6.8: Milstein volatility smile with $(\eta, \kappa, \theta, \rho) = (5, 20, 0.16, -0.5)$.

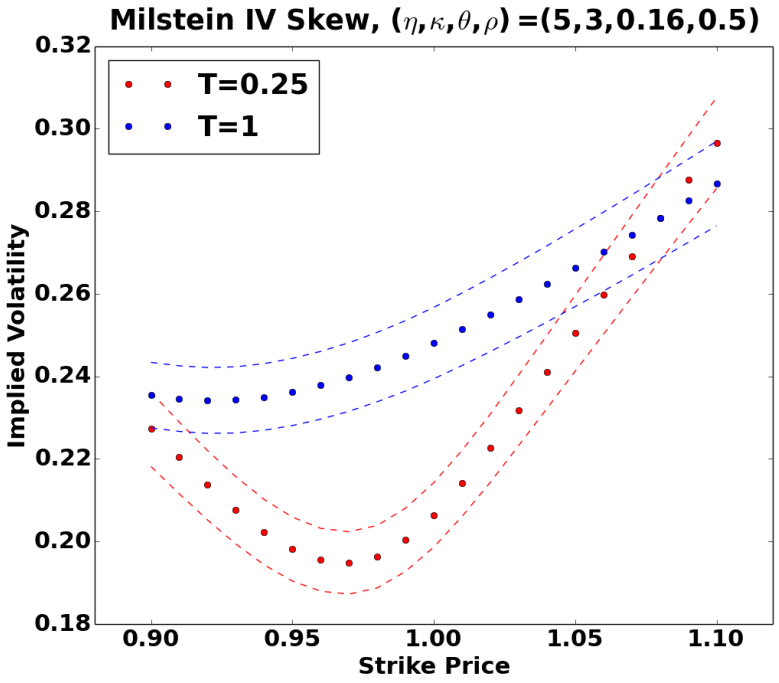

Figure 6.9: Milstein volatility smile with $(\eta, \kappa, \theta, \rho) = (5, 3, 0.16, 0.5)$.

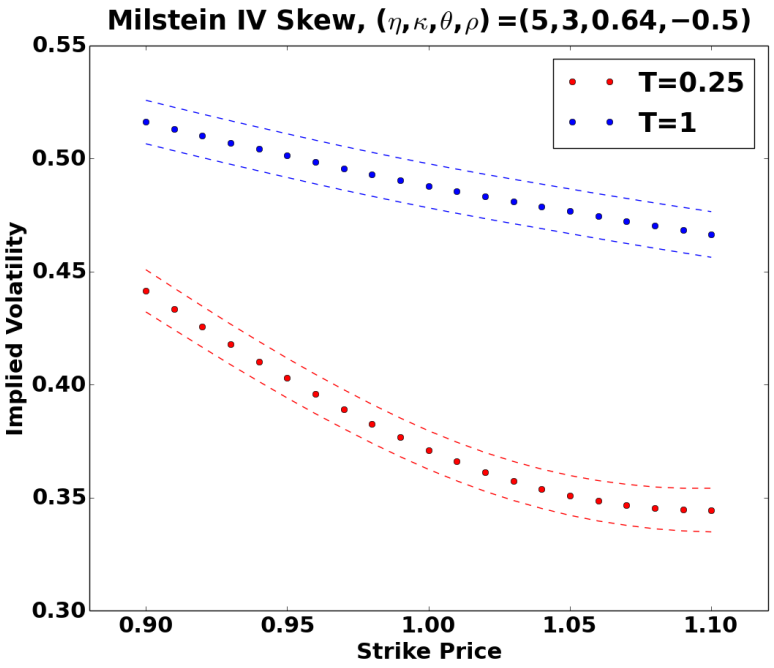

Figure 6.10: Milstein volatility smile with $(\eta, \kappa, \theta, \rho) = (5, 3, 0.64, -0.5)$.

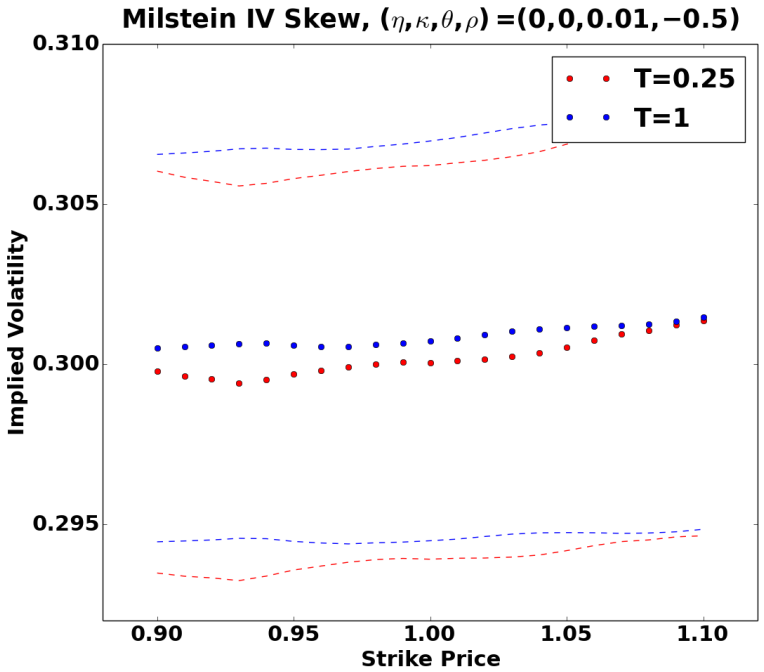

Figure 6.11: Milstein volatility smile with $(\eta, \kappa, \theta, \rho) = (0, 0, 0.01, -0.5)$.

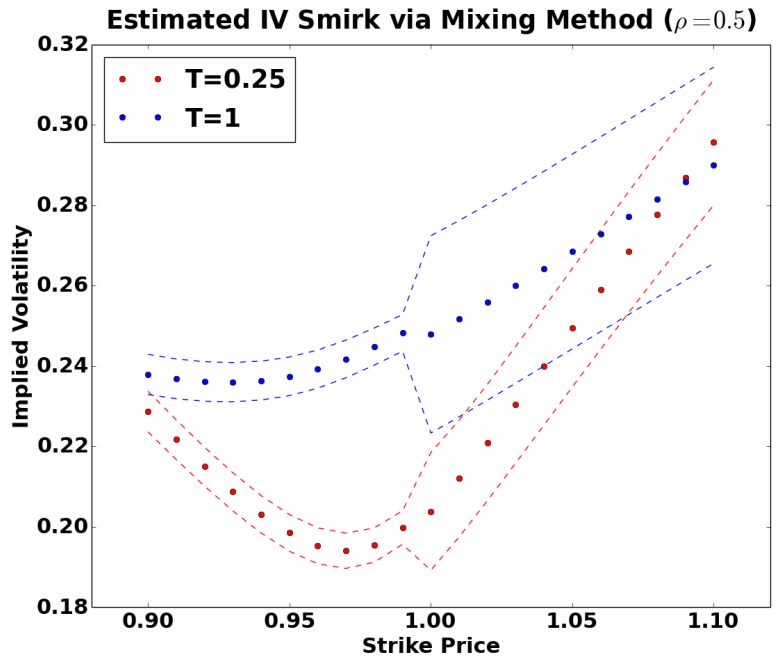

Figure 6.12: Mixing volatility smile with $\rho = 0.5$.

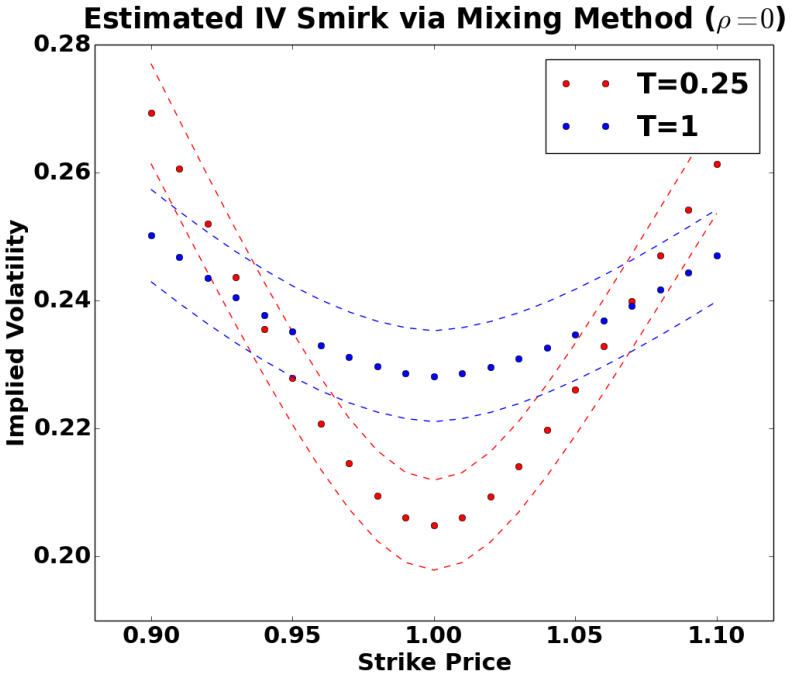

Figure 6.13: Mixing volatility smile with $\rho = 0$.

Bibliography

[Bjork, 1998] Bjork, T. (1998). arbitrage theory in continuous time. *Oxford University Press Inc. New York*.

[Black, 1973] Black, Fischer; Scholes, M. (1973). The pricing of options and corporate liabilities. *Journal of Political Economy*, 81(3):637–654.

[Cox, 1979] Cox, J. C.; Ross, S. A. R. M. (1979). Option pricing: A simplified approach. *Journal of Financial Economics*, 7(3):229.

[Garbow, 1980] Garbow, B. (1980). Documentation for minpack subroutine hybrd: Double precision version.

[James, 2003] James, P. (2003). Option theory. *John Wiley Sons Ltd. West Sussex*.